IEEE Access
Multidisciplinary | Rapid Review | Open Access Journal

Received 17 June 2023, accepted 2 July 2023, date of publication 5 September 2023,
date of current version 19 January 2024.

Digital Object Identifier 10.1109/ACCESS.2023.3312272

RESEARCH ARTICLE

Adaptive Neuro-Fuzzy Damping Controller of Grid-Connected Microgrid Hybrid System Integrating Wind Farms and Batteries

ALIAKBAR HABIBI, BORZOU YOUSEFI, ABDOLREZA NOORI SHIRAZI, AND MOHAMMAD REZVANI
Department of Electrical Engineering, Islamic Azad University, Nour Branch, Nur, Iran
Corresponding author: Borzou Yousefi (borzou.yousefi@iau.ac.ir)

ABSTRACT Renewable energies equipped with LIRs as wind turbines and photovoltaic arrays provide negative impacts on power system dynamic securities. For this issue, developing adaptive controlling strategies play important role on controlling the system dynamic oscillations. In this paper, based on HVDC link, an ANFDC damping controller is proposed for controlling the system dynamic behavior through different LIRs. To do this, a fuzzy linguistic role proposed for tuning ANFDC parameters which the input dynamic signals are transferred into linguistic variables through offline working mode. Then, considering microgrid consists of different LIRs as offshore and onshore WTs, PVs and SSSGs integrated with together, ANFDC is trained which then in online working mode, the system damping performances through different operational and technological structures are evaluated. The proposed scheme is an online and non-model-based controller which uses the advantages of both neural and fuzzy logics together for providing a fast and secure structure of damping controller through online evaluations. The merit and effectiveness of the proposed approach investigated on a grid-connected microgrid consisting of PV, WT and SSSG connected in an incorporated HVDC link which considering different short circuit faults, damping performances are evaluated. Results indicate effectiveness of the proposed scheme for damping dynamic oscillations of LIRs with high damping ratios subject against severe fault events.

INDEX TERMS Low inertia resources (LIRs), high voltage direct current (HVDC), microgrid, wind turbines (WT), photovoltaic arrays (PV), small-scale synchronous generators (SSSGs), adaptive neuro-fuzzy-based damping controller (ANFDC).

I. INTRODUCTION

Due to several issues of operating fossil fuels-based power plant generators through large power system, developing small scale systems known as microgrids equipped by renewable energy sources (RESs) are increasing through today's modern power systems. In this case, wind turbines, photovoltaic arrays and small scale synchronous generators are the most favorable and reliable renewable energy sources which used in the microgrids systems [1].

The associate editor coordinating the review of this manuscript and approving it for publication was Qiang Li.

A. CHALLENGE

Owing with multiple advantages of wind-based power resources, it is known as one of the fixed energy suppliers from 20% penetration level to about several thousand megawatts through topological structures. The corresponding PV and onshore wind turbine sources are known as the second and third RESs through power systems, respectively. However, it should be noting that after 2014, the use of PV-based sources through all of the world passed from WTs in which they reached to about double amounts of WT generations at the end of 2021 [2]. In the case of existing ocean ways, the corresponding wave energies are large and potential RESs with proper energy powers comparing with other RES types.

In this case, countries with the potential of ocean energy resources (e.g. United States, United Kingdom, Denmark, Ireland ...) are increasing rapidly the use of wave energies for producing the electrical power. Considering the amount of ocean surfaces around of the earth, generating the electrical power from offshore wind farms (OWF) and wave energies farm (WEF) can be considered as a potential energy supplier with the advantages of both OWF and WEF suppliers together. In this case, this integration is used properly for generating the power in the England. It is should be noting that developing both OWF and WEF energies require different controlling and protecting schemes which provide several issues through microgrid dynamic security. In this case, due to large amounts of RES powers, there are a set of HVDC links required between the renewable energy resources and the electrical power network [3].

B. LITERATURE REVIEW

Considering developed OWF and WEF sources, the photovoltaic energies known as PV systems can be used as another potential energy integrated with provided RESs which develop the advantage of solar energies in a unit controlling scheme.

1) RECENT RESEARCH EVALUATIONS

Through literature reviews, there are some investigations [4] which provide the advantage of PV systems with respect to other RESs. In [5], it is deducted that the PV schemes require very low maintenance costs, zero pollution, reliable output power and low operational costs with respect to traditional power plants equipped with synchronous generators. Therefore, considering an integrated system consisting of PV, OWF and WEF sources, it is possible to supply considerable amount of generating electrical power with several RES advantages in a unit electrical system [6]. The main idea of providing large RES integrations through power system was initially proposed in [7]. Through simulation results, it was concluded that evaluating the system dynamic oscillations and providing proper controlling system are two important issues which must be investigated through high-level RES penetrations cases. In [8], proportional-integrator-derivative (PID) schemes are proposed as the first damping controllers for adjusting the system critical eigenvalues into secure area. In this case, by evaluating the system critical modes and identifying secure areas, PID controller is provided which the corresponding parameters are adjusted. In [9], considering noisy signal, delay response, nonlinear performance, high cost usage and hard tuning as some problems of PID controllers, a damping controller is proposed. In this reference, model-based PID controller used to provide damping performance through some specific operating cases. In [10], the change of system operating point used to update the PID parameters to reach proper damping performances. Since, power system is a nonlinear and complex system, therefore the conventional linear PID controllers cannot provide proper damping performances which considering the system complexity, PID presents different performances for damping the oscillations [11]. Also, considering PV, WEF, OWF and synchronous generator suppliers in an integrated system, there are different uncertainty and nonlinearity conditions which are resulted from the solar energies, time-variable wind farms, active power oscillations and power electronic switching conditions. In [12], considering large nonlinearities, ANFIS-based PID controllers used to provide damping performance for controlling the system dynamic oscillations. It should be noting that, owing with the controlling designs located at power electronic stations, the provided HVDC links can be used as a virtual damping controller with proper controllability, suitable damping response and significant controlling capacity through interconnected power system [13]. In this case, some intelligent nonlinear techniques including neural network (NN), fuzzy logic (FL) or adaptive neuro-fuzzy inference system (ANFIS) can be used for designing the system wide are damping controller. In [14], considering power system equipped with HVDC links, a NN-based supplementary damping controller is proposed for damping the system dynamic oscillations through interconnected power system. In [15], based on the concept of FL technique, a fuzzy-based damping controller is proposed through power system integrated with HVDC links. Considering the advantages of both NN and FL techniques, a neuro-fuzzy damping controller is proposed in [16] and the system damping response is evaluated through different operating conditions. Results of [12] provide better response with proper damping ratios with respect to damping controllers provided in [17]. Also, the use of flexible AC transmission system (FACTS) are investigated through power system for damping the oscillations. In [18], considering a static VAR compensator (SVC) equipped with ANFIS intelligent technique, the system critical modes are controlled which the developed damping performances are evaluated through different operating condition. In [19], an ANFIS-based damping controller combined with fault detection scheme is developed to provide proper damping performance into power systems with HVDC links.

In [20] and [21], a fuzzy linguistic rule is developed for tuning the parameters which the input signals are transformed into the linguistic variables. In this case, the system dc current error and error ratio are used as two input signals to ANFIS controller.

In [22] and [23], a multi-objective control scheme developed for inverters-based microgrid to control the active and reactive powers through grid-connected topology. Using the reactive current and voltage sequences and line impedance, control structure is developed.

In [24], a controller a mixed linear-adaptive control strategy used for damping the of inter-area oscillation. In this case, considering the inter-area modes formulated as the objective functions, the proposed controller through communication channels developed.

2) RESEARCH GAPS

Through evaluated investigations, most techniques require several cycles with a high dependency on the system model to control the oscillation. In this case, their performances highly depend on the system operational and topological conditions which in the case of changing operating points, updated adjustments are needed. Also, through developing adaptive damping controllers, the use of ANFIS intelligent controllers equipped with HVDC links on inverter/converter sides have not been investigated by the researcher yet.

C. PAPER CONTRIBUTION

In this paper, based on the evaluated recent investigations, an adaptive damping controller scheme is presented.

In this case, the main contributions and novelties of proposed ANFIS-based controller are as follows:

C1-Proposing an adaptive non-model-based ANFIS damping controller in the presence of HVDC links

C2-Using the HVDC link with its individual eigenvalues on modifying the ANFIS tuning parameters.

C3- Considering different RES contributions including PV, WEF, OWF and SSSG incorporated together to evaluate the proposed ANFIS damping performances under different operational and topological structures.

C4- Using the Fuzzy linguistic rule for tuning the ANFIS parameters based on input dynamic signals transformed into the linguistic variables.

C5- Proposing an online scheme based on inverter-based controller to provide ANFIS controlling approach.

C6- Evaluating the proposed damping controller throughout two time-domain and frequency-domain simulations with respect to different operating conditions.

Considering different RES types including PV, WEF, OWF and SSSG, the proposed ANFIS-based damping controller is provided which based on evaluating RES electrical signals under different operating conditions and using the Fuzzy linguistic rule as the main function, the ANFIS damping power are provided. The proposed inverter-based controller is an online and non-model-based scheme which based on providing ANFIS controlling scheme compared with conventional PID controller, the system critical eigenvalues are controlled. The proposed controller is investigated throughout two time-domain and frequency-domain simulations which based on providing different operating conditions, the system dynamic performances are evaluated through inline environment.

D. PAPER ORGANIZATION

The rest of this paper is organized as follows: In Section II, the conceptual structure of the proposed scheme is developed which the corresponding different parts are detailed through different subsections. Section III, considering two ANFIS-based and PID-based damping controller, the designs and detailed structures of the system are presented. The system case study and corresponding simulation results are provided in Section IV. Finally, the paper conclusions and corresponding future research works are provided in Section V.

II. DETAILED STRUCTURE OF THE DEVELOPED TEST SYSTEM

In this section, considering test system consists of different RESs, the structures and dynamic models of developed sources are detailed. The overall view of microgrid test system consists of PV system, WEF, OWF, SSSG connected through HVDC links are illustrated in Figure1.

From Figure 1, the corresponding RESs generate different electrical power which are equipped through individual equipment. In this case, OWF is equipped with a set of permanent magnet synchronous generators (PMSG) which based on wind turbine variable speeds, they can generate 6.5 MW electrical power within nominal operating point. Also, in the case of WEF sources, a set of induction generators are operated in parallel which are linked to wave-based turbines using several gearbox under water. Considering nominal operating point, the corresponding WEF sources can produce 45 MW active power followed through HVDC links. From Figure 1 both WEF and OWF sources are connected through a common bus which considering a HVDC link, the corresponding output electrical powers are transferred to the main grid through common coupling point (CCP) connection. In the case of solar energy, there are a set of PV arrays connected to the test system which the electrical powers are transferred through an equivalent inverter. In nominal operating condition, the corresponding PV system can generate 6.5 MW electrical power which are transferred through installed DC-AC-DC inverters. It is worth noting that each provided RES consist individual dynamic model which should be investigated separately. In this case, considering each of provided RES types, the structure and dynamic models of developed sources are explained and detailed through following subsections. It should be noting that, all of the following mathematical models are presented in p.u system except the model angular frequencies and time variables which are presented in radians/seconds and seconds, respectively.

A. WIND TURBINE MODEL

In an overall description, the output electrical power produced by wind turbine is explained through following description:

$$P_{m\omega}^{OWF} = \frac{1}{2} \times \rho_{\omega} \times A_{r\omega} \times V_{\omega}^{3} \times C_{p\omega}(\lambda_{\omega}, \beta_{\omega}) \quad (1)$$

From (1), ρ_{ω} represents density of the air in kg/m3, $A_{r\omega}$ describe the impacts of blade area in m2, V_{ω} represents the turbine wind speed in m/s and $C_{p\omega}$ explains the wind turbine power coefficient which is defined in dimensionless from as follows:

$$C_{p\omega}(\psi_{k\omega}, \beta_{\omega}) = c_1 \left(\frac{c_2}{\psi_{k\omega}} - c_3 \times \beta_{\omega} - c_4 \times \beta_{\omega}^{c_5} - c_6 \right) \times e^{\left(-\frac{c_7}{\psi_{k\omega}}\right)} \quad (2)$$

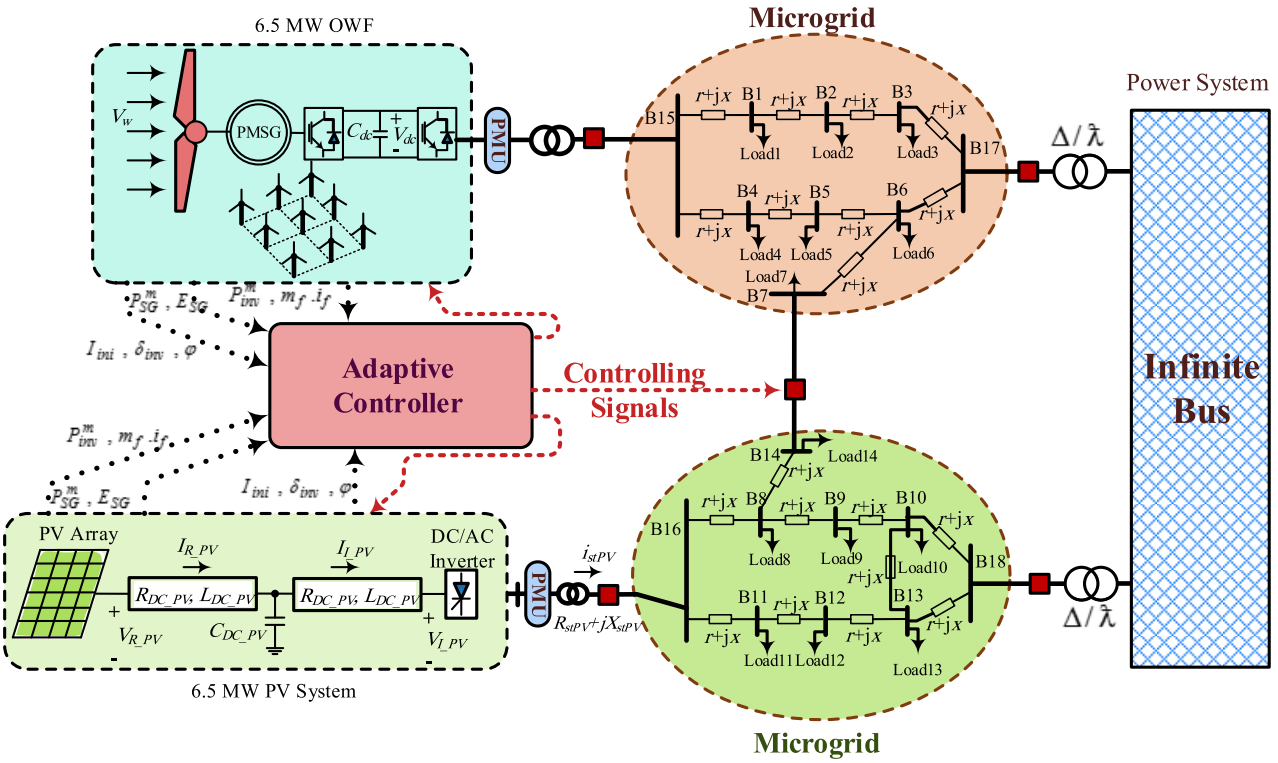

FIGURE 1. Single line diagram of test system consists of PV, WEF, OWF and SSSG sources connected within HVDC link.

From (1) and (2), the parameters λ_ω and $1/\psi_{k\omega}$ are defined as follows:

$$\lambda_\omega = \frac{R_{b\omega} \times \omega_{b\omega}}{V_\omega} \tag{3}$$

$$\frac{1}{\psi_{k\omega}} = \frac{1}{\lambda_\omega + c_8 \times \beta_\omega} - \frac{c_9}{\beta_\omega^3 + 1} \tag{4}$$

From (3) and (4), λ_ω represents the blade speed ratio, $R_{b\omega}$ and $\omega_{b\omega}$ are the blade radius in m and angular speed in rad/second, respectively. β_ω represents the pitch angle of wind turbine blade which is evaluated in degree value. Also, c_1-c_9 are a set of constant coefficients of parameter $C_{p\omega}$ which are specified based on wind turbine speed variables. Based on presented model and considering the wind turbine *cut-in value*=4 m/s, *cut-off value*=25 m/s and *nominal value*=15 m/s, the provided turbine dynamic model is evaluated.

B. WAVE ENERGIES TURBINE MODEL

As definition, considering the wave energy as the input power, the corresponding mechanical power of wave-based turbines can be modeled as follows [8]:

$$P_m^{WEF} = \frac{1}{2}\rho_{WEF} \times A_{rWEF} \times V_{WEF}^3 \times C_{pWEF}(\lambda_{WEF}, \beta_{WEF}) \tag{5}$$

From (5), ρ_{WEF} represents density of the water in kg/m3, A_{rWEF} is the turbine blade area in m^2, V_{WEF} is the turbine velocity in m/s and C_{pWEF} represents a constant coefficient evaluated from turbine speed ratio λ_{WEF} and pitch angle β_{WEF}, correspondingly. Based on provided model (5) and considering *cut-in value*=1m/s, *cut-off value*= 5 m/s and *rated value*=2.5 m/s, the provided wave-based turbine dynamic model is evaluated.

C. PERMANENT MAGNET INDUCTION GENERATOR (PMSG) EQUATIONS FOR WIND TURBINE MODEL

Through provided OWF models, wind turbines are equipped with a set of PMSG models. In this case, considering Park equations through *d-q* axis, the corresponding PMSG models can be described as follows [25]:

$$p(\phi_{qw}) = (\omega_b \times \upsilon_{qsw}) + (\omega_b \times r_{sw} \times i_{qsw}) - (\omega_{rw} \times \phi_{dw}) \tag{6}$$

$$p(\phi_{dw}) = (\omega_b \times \upsilon_{dsw}) + (\omega_b \times r_{sw} \times i_{dsw}) - (\omega_{rw} \times \phi_{qw}) \tag{7}$$

From (6) and (7), υ_{sw} and i_{sw} are the voltage and current values of stator windings evaluated in p.u scale, respectively. ω_{rw} represents the PMSG rotor speed in radian/s. Also, ϕ_{qw} and ϕ_{dw} represent the generator flux leakages which are defined as follows:

$$\phi_{qw} = -(X_{mqw} + X_{lsw})\, i_{qsw} = -(X_{qw} \times i_{qsw}) \tag{8}$$

$$\phi_{dw} = -(X_{mdw} + X_{lsw})\, i_{dsw} + X_{mdw} i'_{mw} = -(X_{dw} \times i_{dsw}) + (X_{mdw} \times i'_{mw}) \tag{9}$$

From (8) and (9), X_{lsw} and X_{mw} are the generator leakage and magnetization reactance evaluated in p.u and is

the generator magnetization current. Considering a voltage source converter (VSC) connected between wind turbine and PMSG generator, the corresponding output voltages υ_{condw} and υ_{conqw} in d-q axis evaluated through p.u scales are defined as follows:

$$\upsilon_{condw} = km_{condw} \times \upsilon_{dcw} \tag{10}$$

$$\upsilon_{conqw} = km_{conqw} \times \upsilon_{dcw} \tag{11}$$

From (10) and (11), km_{condw} and km_{conqw} are two constant coefficients defined based on VSC converter side values and υ_{dcw} is the dc voltage of VSC-link. Considering developed model, the output voltages of inverter side VSCs provided from PMSG sources are defined as follows:

$$\upsilon_{invdw} = km_{invw} \times \sin(\alpha_{invw}) \times \upsilon_{dcw} \tag{12}$$

$$\upsilon_{invqw} = km_{invw} \times \cos(\alpha_{invw}) \times \upsilon_{dcw} \tag{13}$$

From (12) and (13), km_{invw} and α_{invw} are the constant coefficient and phase angle evaluated from VSC inverter side, respectively. Detailed structure related to VSC through both converter and inverter sides are given in [26]. From provided VSC model, km_{invw} controls the PMSG reactive power Q_w, phase angle α_{invw} is designed to control the PMSG speed deviations ω_{rw}, two constant coefficient km_{condw} and km_{conqw} are responsible to evaluate and control the SVC dc-link υ_{dcw} and stator voltage υ_{sw}, respectively.

D. INDUCTION GENERATOR (IG) EQUATIONS FOR WAVE ENERGY-BASED TURBINE MODEL

From Figure 1, there are a set of wave-based turbine models which generate the input mechanical power to connected induction generators. In this case, considering d-q Park equations, the voltage and current formulation of provided induction generators are defined as follows [16] and [27]:

$$\frac{\left[(X_{ls}+X_m)\times p(i_{qs})\right]-\left[(X_m)\,p(i_{qr})\right]}{\omega_b} = -\left(r_s\times i_{qs}\right)-\left(\omega_e\,(X_{ls}+X_m)\,i_{ds}\right)+\left(\omega_e X_m i_{dr}\right)-\upsilon_{qs} \tag{14}$$

$$\frac{[(X_{ls}+X_m)\times p(i_{ds})]-[(X_m)\,p(i_{dr})]}{\omega_b} = -\left(r_s\times i_{ds}\right)+\left(\omega_e\,(X_{ls}+X_m)\,i_{qs}\right)-\left(\omega_e X_m i_{qr}\right)-\upsilon_{ds} \tag{15}$$

$$\frac{\left[(X_{lr}+X_m)\times p(i_{qr})\right]-\left[(X_m)\,p(i_{qs})\right]}{\omega_b} = -\left(r_r\times i_{qr}\right)+\left((\omega_e-\omega_r)\,(X_m i_{ds})\right)-\left((\omega_e-\omega_r)\,(X_{lr}+X_m)\,i_{dr}\right) \tag{16}$$

$$\frac{[(X_{lr}+X_m)\times p(i_{dr})]-[(X_m)\,p(i_{ds})]}{\omega_b} = r-\left(r_r\times i_{dr}\right)-\left((\omega_e-\omega_r)\,(X_m i_{qs})\right)+\left((\omega_e-\omega_r)\,(X_{lr}+X_m)\,i_{qr}\right) \tag{17}$$

From (14)-(17), r_s and r_r represent the stator and rotor winding resistances. X_{ls} and X_m are the leakage and magnetization reactance, respectively. υ_{ds}, υ_{qs}, ids and i_{qs} are the induction generator stator voltages and currents in d-q axis, respectively. i_{dr} and i_{qr} are the induction generator rotor currents in d-q axis, respectively. ω_e, ω_r and ω_b are the generator angular, rotational and reference speeds, respectively. Finally, considering the system currents and voltages, the input electromechanical torque T_e of induction generator is evaluated as follows:

$$T_e = X_m\left[\left(i_{dr}\times i_{qs}\right)-\left(i_{qr}\times i_{ds}\right)\right] \tag{18}$$

E. HVDC-LINK MATHEMATICAL MODEL

Based on provided model in Figure 1, the corresponding HVDC-link is equipped through three different parts including 1-AC/DC converter, 2-dc-link and 3-DC/AC inverter which is designed in a unified structure known as HVDC link model [18], [28]. It should be noting that for providing proper performances, the HVDC ac and dc parameters should be estimated properly. For this issue, in the case of converting the electrical power from dc pu scale to reference value in ac part, the corresponding HVDC dc parameters must be remained unchanged [29]. The corresponding mathematical equations related to above provided descriptions are given in [18] and [29]. Detailed structures of the developed HVDC current rectifier (CRHVDC) and HVDC current inverter (CIHVDC) are illustrated in Figure 2 and Figure 3, respectively.

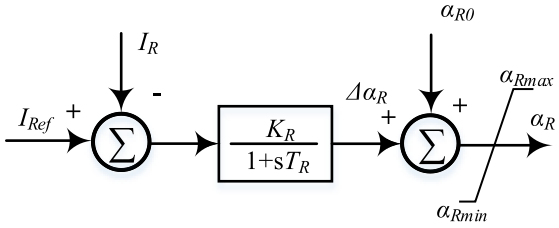

FIGURE 2. Controlling block diagram of the HVDC current converter.

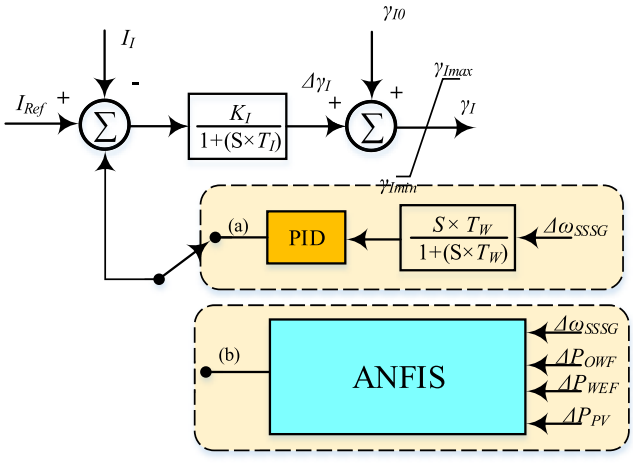

FIGURE 3. Controlling block diagram of the HVDC current inverter including (a) PID controller and (b) ANFIS controller.

From Figure 2 and Figure 3, the developed HVDC current parameters CRHVDC and CIHVDC are calculated as

follows:

$$(T_R)\, p\,(\alpha_R) = K_R\left(I_{Ref} - I_R\right) - \alpha_R \tag{19}$$

$$(T_I)\, p\,(\gamma_I) = K_I\left(I_{Ref} - I_I + I_C\right) - \gamma_I \tag{20}$$

From (19) and (20), I_C is the controller damping signal which is obtained by two developed PID and ANFIS damping controllers through different operating conditions. Detailed structures of the developed controllers are presented in Section III through different mathematical formulations.

F. PV FARM MATHEMATICAL MODEL

In the case of PV system, considering a set of BP272UU panel types with the nominal powers of 80 watts, nominal voltages of 19 volts, nominal currents of 4.4 amperes, short circuit currents of 4.6 amperes and open circuit voltages of 21.5 volts, the corresponding PV arrays are designed. Owing to low voltages of PV panels, considering a set of PV series structures linked together, proper output voltage is provided. In the case of protecting PV panels against environment issues, considering a set of panels with transparent encapsulated materials (e.g. plastic, glass and so on), PV arrays are provided. Also, in order to obtain proper current and corresponding power, a set of PV panels are linked in parallel together which the required output powers are provided. Totally, considering 400,000 PV panels connected through series and parallel structures, there are 6.5 MW as the output electrical powers from developed PV farms. Single line circuit of the PV panels developed through parallel structures is shown in Figure 4.

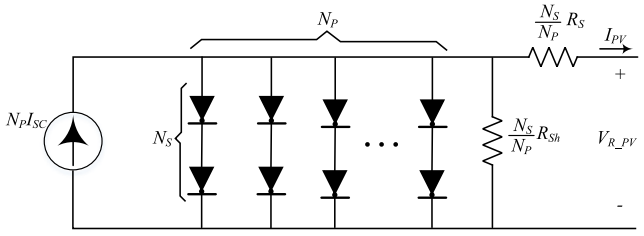

FIGURE 4. Single line diagram of PV parallel structure.

From Figure 4, $N_p I_{SC}$ represents the PV model short circuit current source which is connected in parallel with N_s series and N_p parallel diodes and one shunt resistor R_{sh} in a unified circuit line structure. Considering provided current model, the equivalent PV current IPV is evaluate as follows:

$$I_{PV} = N_P I_{SC} - N_P I_D\left(e^{\left[\frac{q}{A\times k\times T}\left(\frac{V_{R-PV}}{N_S} + \frac{R_S I_{PV}}{N_P}\right)\right]-1}\right) - \frac{N_P}{R_{sh}}\left(\frac{V_{PV}}{N_S} + \frac{R_S I_{PV}}{N_P}\right) \tag{21}$$

From (21), V_{R-PV} represents the output voltage of PV arrays, q and k and A are the electron, Boltzmann and quality factor constants including q =-1.602 $\times$ 10^{-19} C and k =1.38 $\times$ 10^{-23} J/K, respectively. Also, T represents the ambient temperature, I_D and I_{SC} are the diode reverse and short circuit currents under reference solar radiations as 1000 W/m2. The single line diagram of the PV system dc lines and corresponding DC/AC inverters are illustrated in Figure 5.

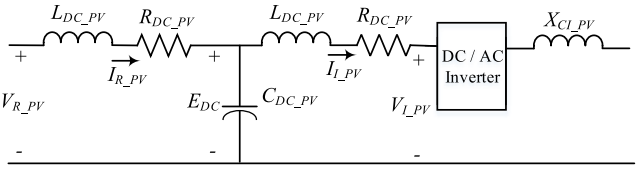

FIGURE 5. PV system circuit consists of dc line and DC/AC inverter.

From Figure 5, CDC-PV is used as the PV battery system which is located in parallel at the center point of provided PV model. Considering developed current source model, the PV system differential formulations are developed as follows:

$$(L_{DC-PV})\, p\,(I_{R-PV}) = V_{R-PV} - (R_{DC-PV} \times I_{R-PV}) - E_{DC} \tag{22}$$

$$(C_{DC-PV})\, p\,(E_{DC}) = I_{R-PV} - I_{I-PV} \tag{23}$$

$$(L_{DC-PV})\, p\,(I_{I-PV}) = E_{DC} - V_{I-PV} - (R_{DC-PV} \times I_{I-PV}) \tag{24}$$

From (22)-(24), the output voltage of PV in inverter side is defined as follows:

$$V_{I-PV} = \sqrt{\frac{V_{qINV-PV}^2 + V_{dINV-PV}^2}{2}}\cos\left(\gamma_{I-PV}\right) - \frac{\pi}{6}\left(X_{CI-PV} \times I_{I-PV}\right) \tag{25}$$

The block diagram of the PV system current control scheme developed through DC/AC inverter is provided in Figure 6.

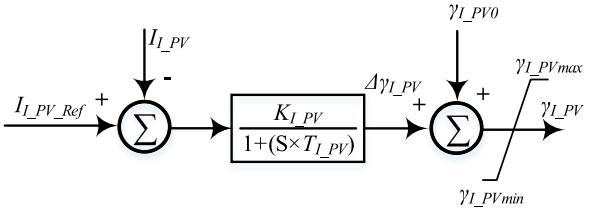

FIGURE 6. PV system current control scheme.

Considering Figure 6, the corresponding differential formulation through DC/AC inverter is expressed as follows:

$$T_{I-PV} p(\gamma_{I-PV}) = K_{I-PV}\left(I_{I-PV-ref} - I_{I-PV}\right) - \gamma_{I-PV} \tag{26}$$

G. SSSG DIFFERENTIAL MODEL

In the case of synchronous generator model, considering a well-known third order differential model presented in [32], the corresponding microgrid SSSGs are developed. The system descriptions consist of SSSG differential formulations in d-q axis and corresponding single line equivalent circuits are described in detail in [32]. All provided SSSGs are equipped

with an IEEE type DC1A excitation system which control the generator internal voltage through different operating points [16], [27]. Detailed information related to provided excitation systems are given in the Appendix. For evaluating the developed SSSGs through transient and sub-transient fault conditions, considering the following three assumptions, SSSG dynamic behaviors are evaluated:

Assume 1) The provided differential equations are scaled into d-q frame which the corresponding time-dependent issues are fixed through rotor speed rotations.

Assume 2) The generator rotor sides consist two different windings through each dq axis. In this case, the system d axis side is equipped with one damping and one filed winding while there are two damping windings on the q axis frame.

Assume 3) Transient effects of the generator stator windings are ignored through provided differential equations and corresponding output voltage signals.

III. MODELING THE PROPOSED DAMPING CONTROLLER

In this section, considering provided HVDC link equipped with two individual ANFIS and PID damping controllers, the corresponding different parts are described. Conceptual structure of the proposed ANFIS-based damping controller is provided in Figure 7.

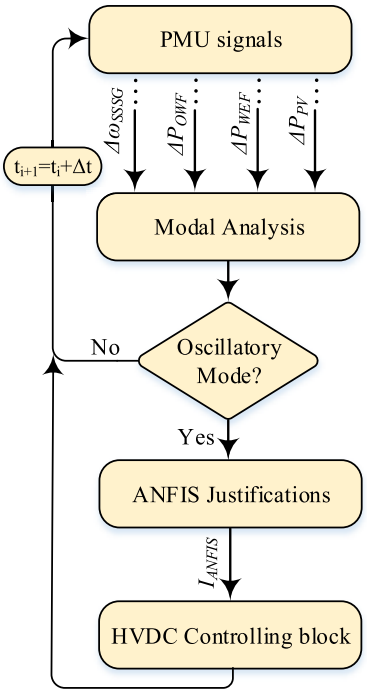

FIGURE 7. Conceptual structure of the proposed ANFIS-based controlling scheme.

In real-time environment, based on the microgrid operating point, the system oscillatory modes are varied. In this case, considering different fault event types, some individual oscillatory modes are excited which lead to different oscillation frequencies with individual damping ratios. For this issue, by online evaluations of the system dynamic security, the system critical oscillatory modes must be identified which the corresponding controlling actions should be estimated. From Figure 7, based on PMU signals and developing the modal analysis through frequency domain, the system dynamic security is evaluated. In this case, by using the developed controller, the extinction angle of the HVDC links on the inverter side is estimated. Also, considering speed deviations of synchronous generators $\Delta\omega_{SSSG}$ as the input signals to the controller, the corresponding damping signals is provided in which the identified system oscillatory modes are controlled. Also, in the case of training ANFIS controller, considering the system dynamic behaviors equipped with PID controller through severs fault disturbances, the corresponding dynamic responses are evaluated which is used as input data for organizing the ANFIS controller through time-domain simulations. In this case, at each operating point, a set of fault disturbances with the potential of severe dynamic oscillations are evaluated which considering four different dynamic signals including (a) SSSG speed deviations $\Delta\omega$, (b) Active power deviations of the system OWF generators ΔP_{OWF}, (c) Active power deviations of the system WEF generators ΔP_{WEF} and (d) Active power deviations of the system PV arrays ΔP_{PV}, as input data to ANFIS controller, the corresponding intelligent structure is trained. It should be noting that considering four dynamic variables as input signals provide more complicated processes and time consumptions through offline evaluations. However, in the case of proper training processes, the proposed ANFIS damping controller are able to provide proper damping response with high damping ratio through different operating conditions.

A. MODELLING PID CONTROLLER THROUGH HVDC LINK MODEL

In this section, the procedure and structure of the proposed PID controller is presented. Based on controlling diagram presented in Figure 3, the provided HVDC link consists one PID damping controller which uses the SSSG speed deviations $\Delta\omega_{SSSG}$ as input signal for controlling the system dynamic behaviors. In order to design the controller structure, based on developing modal analysis, the system eigenvalues and corresponding oscillatory modes are evaluated.

For this issue, considering typical operating point (OP), $OP1$=13 m/s, $OP2$=3 m/s and PV output current I_{PV} within solar radiation of 1000 W/m2, the proposed PID controller is developed. In this case, considering modal analysis through frequency-domain, the corresponding microgrid eigenvalues and the system damping performances with and without presenting PID controller are evaluated.

It should be noted that based on the system topological structure, each RES model (e.g. HVDC Link, SSSG, PID controller) modeled as individual eigenvalues into the system which play different role on damping the oscillation. Under eigenvalue analysis, it is possible to evaluate the RES eigenvalues and their controlabilities on damping the oscillation. In Table 1, considering individual eigenvalues of different

RESs, effectiveness of the proposed damping controller on controlling individual eigenvalues are evaluated.

The system eigenvalue real and image parts evaluated from two different controlling cases (i.e. (a) Without activating PID controller, (b) Activating PID controller) are illustrated in Table 1.

TABLE 1. Eigenvalue analysis of the test system with and without proposed PID damping controller.

Eigenvalue Num.	RES	Eigenvalue specifications			
		Real Part		Image Part	
		Without	With	Without	With
$\lambda_{1\text{-}2}$	OWF	-15.56	-15.67	3.42 e+6	3.35 e+6
$\lambda_{3\text{-}4}$		-15.08	-15.23	3.72 e+6	3.84 e+6
$\lambda_{5\text{-}6}$		-2.51	-2.69	5.71	5.66
λ_{7}		-99.3	-99.4	0.00	0.00
λ_{8}		-100.8	-100.85	0.00	0.00
λ_{9}		-0.45	-0.46	0.00	0.00
$\lambda_{10\text{-}11}$	WEF	-54.51	-54.78	25.23 e+2	25.36 e+2
$\lambda_{12\text{-}13}$		-118.21	-118.32	17.13 e+2	17.18 e+2
$\lambda_{14\text{-}15}$		-175.2	-175.56	965.2	965.2
λ_{16}		-163.1	-163.19	0.00	0.00
$\lambda_{17\text{-}18}$		-3.02	-3.15	4.26	4.26
$\lambda_{19\text{-}20}$	HVDC Link	-736.2	-736.13	91.32 e+2	91.45 e+2
$\lambda_{21\text{-}22}$		-501.3	-501.21	63.12 e+2	63.56 e+2
$\lambda_{23\text{-}24}$		-312.4	-312.42	24.56 e+2	24.87 e+2
λ_{25}		-18.8	-18.88	0.00	0.00
λ_{26}		-10.1	-10.16	0.00	0.00
$\lambda_{27\text{-}28}$	PV	-131.5	-131.68	78.13	79.27
$\lambda_{29\text{-}30}$		-36.3	-36.42	43.14	43.21
$\lambda_{31\text{-}32}$		-1.54	-1.67	1.03	1.05
$\lambda_{33\text{-}34}$	SSSG	-25.14	-25.29	89.15 e+2	89.39 e+2
$\lambda_{35\text{-}36}$		-32.12	-32.33	87.62 e+2	87.27 e+2
$\lambda_{37\text{-}38}$		-0.61	-0.66	367.9	368.4
λ_{39}		-33.71	-33.85	0.00	0.00
$\lambda_{40\text{-}41}$		**-0.012**	**-1.63**	**9.65**	**10.21**
$\lambda_{42\text{-}43}$		-8.82	-8.85	10.75	10.98
λ_{44}		-15.64	-15.68	0.00	0.00
$\lambda_{45\text{-}46}$		**-0.016**	**-2.24**	**6.32**	**6.97**
λ_{47}	PID Controller	---	-23.02	---	0.00

From Table 1, it is indicated that through evaluated microgrid modes, the eigenvalue numbers λ_{40-41} and λ_{45-46} are the known as critical oscillatory modes in the range of low frequency oscillations (i.e. f=1-5 Hz) which present the lowest damping ratios with respect to other eigenvalues. It should be noting that through evaluated eigenvalues, there are other oscillatory modes (e.g. λ_{37-38}). Owing to evaluated high frequency ratios, the corresponding mode's amplitudes are damped much faster than low-frequency oscillatory modes. Therefore, based on the frequency evaluations, eigenvalues with the frequencies higher than specified frequency are not considered through controlling procedure for designing PID damping controller. It should be noting that the main aim of developing damping controllers is to provide proper damping performance of developed HVDC links in the presence of renewable energy resources including OWF, WEF, PV and SSSG generators. For this issue, based on RESs operating points, there are eigenvalue parameters with different oscillatory specifications. In this case, at each time window, by evaluating the modal analysis through system steady state matrix, critical modes are identified in which the corresponding adjustments are implemented through developed damping controllers. Considering Figure 3, the provided PID controller consist of a first order washout block which filters the noises to provide proper input signal illustrating the system dynamic oscillations. In this case, considering speed deviations of SSSGs $\Delta\omega_{SSSG}$ as input data, the corresponding damping signal I_C is provided to improve damping ratio of identified oscillatory modes λ_{40-41} and λ_{45-46} illustrated in Table 1. Based on Figure 3, the corresponding PID damping signal IC is compared with the reference signal I_{ref} which provide proper damping signal in phase with the occurred low frequency oscillations. For this issue, considering $H(s)$ as the main transfer function of developed PID controller, the corresponding eigenvalues are controlled. In this case, considering $\Delta\omega_{SSSG}$ and I_C as the input-output pair's data, the corresponding PID controller transfer function is provided as follows:

$$H_{PID}(S) = \frac{I_C}{\Delta\omega_{SSSG}} = \frac{S \times T_W}{1 + S \times T_W}\left(K_P + \frac{K_I}{S} + (S \times K_D)\right) \quad (27)$$

From (27), TW represents time constant of the PID washout filter. Also, K_P, K_I and K_D represent the proportional, integrator and derivative coefficient factors of the PID controller which are specified based on the expected damping ratios, respectively.

It should be noting that through real-time evaluations, at each time window Δt, considering modal analysis through the microgrid dynamic state variables, the system critical eigenvalues are identified which by substituting the PID transfer function through system steady state matrix and evaluating the PID four unknown parameters T_W, K_P, K_I and K_D with respect to critical modes, proper values with the aim of high damping ratios are provided. Model analysis results of the test system considering PID controller transfer function is provided in Table 2.

TABLE 2. Modal analysis results considering PID parameters through main system closed loop transfer function.

Eigenvalue Num.	Eigenvalue specifications			
	Real Part		Image Part	
	Without	With	Without	With
$\lambda_{40\text{-}41}$	**-0.012**	**-1.63**	**9.65**	**10.21**
$\lambda_{45\text{-}46}$	**-0.016**	**-2.24**	**6.32**	**6.97**

PID Parameters	K_P	K_I	K_D	T_W
	-0.62	34.71	0.19	0.38 s

From Table 2, considering PID controlling parameters through the system closed loop transfer function, the specified critical modes λ_{40-41} and λ_{45-46} are controlled properly which the corresponding real parts are moved to secure area within proper damping ratios. In this case, the corresponding damping ratios are improved from -0.012 and -0.016 without considering PID controller to -1.63 and -2.24 in the presence of PID controller, respectively. Detailed description and corresponding constraints related to identifying proper PID parameters are expressed in [33]. Considering modal analysis results evaluated from closed loop transfer function, it is concluded that the provided PID controller presents proper damping response through test system which the corresponding critical modes are located within secure area using specified damping parameters.

B. MODELLING ANFIS DAMPING CONTROLLER THROUGH HVDC LINK MODEL

In this section, procedures and detailed structures of the proposed ANFIS damping controller is expressed. For this issue, considering a Sugeno ANFIS type, the corresponding different parts are provided through following subsections:

1) CONCEPTUAL STRUCTURE OF ANFIS MODEL

The structure and organization of developed ANFIS-based damping controller is based on the Sugeno type [34], [35] which is a well-known method of estimating controller parameters in the presence of different uncertainties. Through proposed Sugeni-ANFIS model, the fuzzy logic (FL) and neural network (NN) structure are designed as model-free type which provide both advantages of FL and NN models with respect to input signal noises and uncertainties. In this case, the input data are encoded within a set of distributed parallel framework which are evaluated through numerical analysis. By this way, the corresponding FL and NN logics can be converted together within the same architectures. Also, in the case of providing FL and NN models through a unified structure, it is possible to develop a comprehensive training procedure with good architecture which identify proper damping parameters through real-time evaluations. It should be noting that unlike the conventional NN structures presented as different black-box frameworks, the proposed ANFIS final architecture is developed through a set of intelligent fuzzy logics based on provided dynamic variables [36]. In this case, the ANFIS structure is formed into two separate parts like FL framework. The first part of developed ANFIS controller presents the system antecedent data which is used for predicting proper decision while the second part consists the conclusion data which works as feedback signal to modify estimated decisions. The corresponding ANFIS parts are worked together through a unified structure which based on provided fuzzy roles, proper estimations are provided. In the case of developing five individual layers through ANFIS architecture, it is known as multilayer NN framework as illustrated in Figure 8.

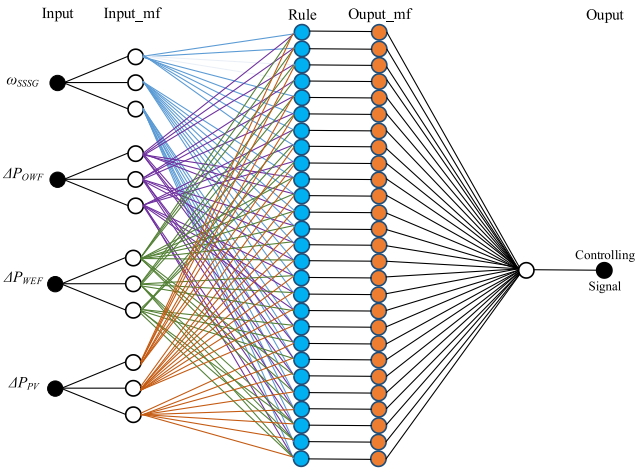

FIGURE 8. Neural network multilayer structure through ANFIS framework.

From Figure 8, ANFIS architecture consists of five individual layers presenting different roles through intelligent processes. In this case, based on presented input signals, a fuzzification procedure is processed in the first layer (i.e. input) which the input signals are encoded through a set of fuzzy roles. In the second layer (i.e. inputmf), based on provided fuzzification results, the fuzzy roles and corresponding antecedent logics are executed. The third layer (i.e. rule) is responsible to normalize the ANFIS membership functions through a set of AND logics which based on evaluated signals, proper decisions are estimated. Considering estimated roles, the corresponding decoding processes and conclusion part are provided through the fourth layer (i.e. outputmf). Finally, based on evaluated conclusions, the corresponding outputmf summations are provided through the last layer (i.e. output). In this case, based on microgrid test system and ANFIS architecture developed in Figure 8, four dynamic variables including $\Delta\omega$SSSG, ΔPOWF, ΔPWEF and ΔPPV are considered as input signal to ANFIS damping controller. Considering Figure 7, the structure and fuzzification roles of provided Sugeno-based ANFIS architecture is expressed as follows:

$$\begin{aligned} &\textit{If} \\ &(x_1 = A_i)\ \textit{AND}\ (x_2 = B_i)\ \textit{AND}\ (x_3 = C_i)\ \textit{AND}\ (x_4 = D_i) \\ &\textit{then} \\ &(f_i = p_i x_1 + q_i x_2 + r_i x_3 + y_i x_4 + s_i) \end{aligned} \tag{28}$$

From (28), parameters x_1-x_4 represent the ANFIS input variables, A_i, B_i, C_i and D_i are the input variables fuzzification sets. Also, fi represents the corresponding ANFIS output signal and parameters p_i, q_i, r_i, y_i and s_i are the fuzzy logic parameters which are specified adaptively during the ANFIS training procedure through ith numbers of membership function with respect to determined input signal.

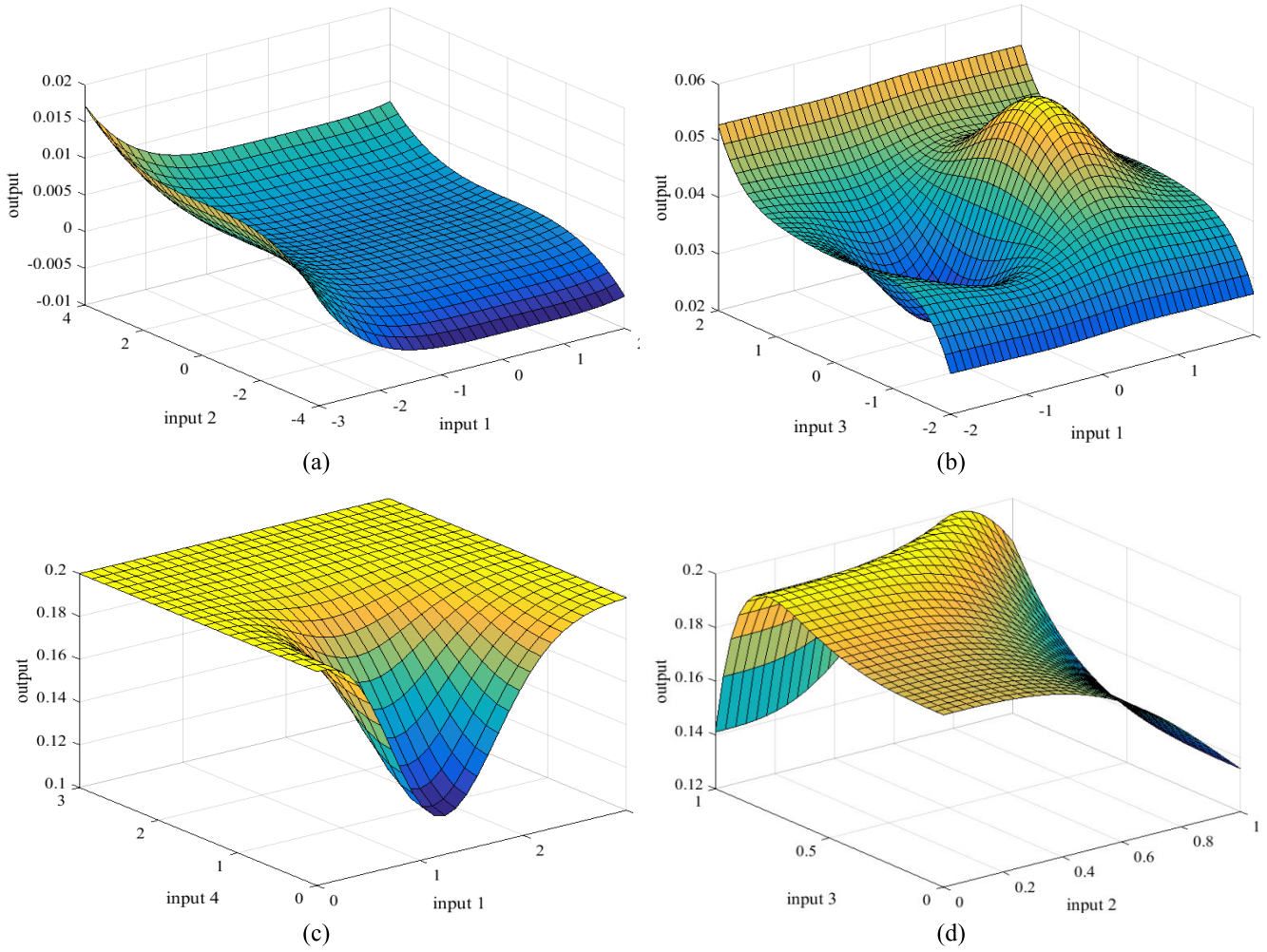

FIGURE 9. The ANFIS fitting curve and surface plot with respect to different input combinations.

2) ANFIS TRAINING PROCEDURE

The corresponding training procedure of proposed PID and ANFIS damping controllers are based on fuzzy role consists of input-output pairs data for training and tuning the parameters. In this case, a linguistic rule [20], [21] is developed which the input signals are transformed into the linguistic variables. The corresponding controller surface to show data training qualities are developed in Figure 9. Based on the simulation evaluations, input-output pairs signals are used to ANFIS structure in which the corresponding fuzzification roles are learned. In this case, considering each input-output pairs data, the ANFIS membership functions are provided similar to artificial neural network structures. This is the main training procedure of the proposed Sugeno-based ANFIS algorithm. Considering provided procedure, a hybrid multifunction training procedure is developed to identify ANFIS parameters which the corresponding fuzzification roles are estimated. Also, in order to estimate damping parameters, considering combined least-square (LS) and back-propagations gradient decent (BPGD) techniques as the main function and comparing the ANFIS estimations with investigated simulation results, the corresponding ANFIS membership functions are trained through offline evaluations.

3) DETAILED STRUCTURE OF THE DEVELOPED ANFIS CONTROLLER

In this section, considering the ANFIS controlling block provided in Figure 3, the procedure and detailed structure of damping controller is expressed. For this issue, based on renewable energy resources provided in Section II, speed deviations of small-scale synchronous generators $\Delta\omega_{SSSG}$, wind turbine active power deviations ΔP_{OWF}, wave turbine active power deviations ΔP_{WEF} and PV arrays active power deviations ΔP_{PV} are determined as input dynamic signals to proposed ANFIS damping controller. In the case of determining input signals, evaluating modal analysis results through provided electromechanical signals show that they are able to illustrate the system low-frequency oscillations with proper observability index during different operating conditions.

Based on the type and location of the fault event occurrences, the system dynamic oscillations are used as input signal to ANFIS damping controller which considering the provided membership functions, proper controlling signals IC in phase with the identified oscillatory modes λ_{40-41} and λ_{45-46} are provided. It should be noting that all of training and evaluating processes of proposed ANFIS damping controller are utilized using powerful ANFIS framework employed through MATLAB@. Through developed model, the fuzzy-based membership functions and corresponding NN layers are fixed into ANFIS structure which based on evaluated signals, proper decisions are estimated. In the case of evaluating a set of input-output pairs data through developed model, the corresponding fuzzy membership functions (i.e. fuzzification and defuzzification processes) are performed through a set of parametric models which the corresponding parameters are estimated using neural network multilayer processes. Actually, this is a deduction form of conventional fuzzy logic model which is known as ANFIS system consists of both fuzzy and neural network through a unified closed loop structure. In this case, considering each input dynamic variable, the ANFIS fuzzy model consists of 344 different roles through seven membership functions to provide proper performance within different dynamic oscillations. The corresponding seven input membership functions (IMFs) through input variables are included as follows:

IMF1: Negative Big (NB), IMF2: Negative Medium (NM), IMF3: Negative Small (NS),

IMF4: Zero (Z),

IMF5: Positive Small (PS), IMF6: Positive Medium (PM) and IMF7: Positive Big (PB).

There are also seven output membership functions (OMFs) through output dynamic variables which are included as follows:

OMF1: Increase Big (IB), OMF2: Increase Medium (IM), OMF3: Increase Small (IS),

OMF4: Hold (H),

OMF5: Decrease Small (DS), OMF6: Decrease Medium (DM) and OMF7: Decrease Big (DB).

Considering provided IMFs and OMFs functions, the RESs dynamic signals are used through four input variables into ANFIS controlling structure. The main aim of developing different membership functions is to provide proper small rules through following ANFIS training procedure:

- Generating the input-output pairs data: In order to provide proper ANFIS structure, a set of input date and corresponding output concluded estimations are required. In this paper, considering each sampling data evaluated form simulation studies, a four-dimensional input signal (IS) including $\Delta\omega_{SSSG}$, ΔP_{OWF}, ΔP_{WEF}, ΔP_{PV} and corresponding one-dimensional controlling signal (CS) as IC are considered for training the proposed ANFIS damping controller.

- Extracting the rules of Membership functions: In the case of generating input-output data, the next part is to evaluate the ANFIS structure through developed signals to provide initial MFs. For this issue, considering subtractive clustering (SC) technique provided in [21], the ANFIS initial rules and corresponding MFs are extracted. It should be noting that during the initial evaluations, the corresponding initial rules are not close to optimize parameters. Therefore, an online optimization procedure is required to tune the rules close to identified proper values. In this case, after providing initial rules evaluated from SC algorithm, a hybrid training algorithm (HTA) is utilized for training ANFIS system to provide proper controlling parameters. The corresponding HTA scheme consists two different algorithms for optimizing the MFs and resultant equation parameters. In this case, by using back-propagation algorithm (BPA) the ANFIS membership functions are tuned during different iterations. Next, considering the least-square optimization technique (LSOT), the system resultant equation parameters are optimized. The corresponding optimization procedure is continued iteratively until a constant error is evaluated.

- Estimated predictions: In order to evaluate estimated predictions, a set of nonlinear evaluations are employed through provided ANFIS system. In this case, considering different nonlinear processes through developed rules and transfer functions, damping performance of provided ANFIS controller are evaluated. It should be noting that the main aim is to provide ANFIS structure through the lowest fuzzy rule numbers with the same damping performance (i.e. lower then 50 ruls). In order to illustrate the system effectiveness through fuzzy rules, considering two different cases including (a) Lower case with 30 rules and (b) Optimized case with total required rules, the system dynamic performances are evaluated. By identifying the lowest required fuzzy rules, the system computation times and the corresponding required memories will be decreased.

Based on Figure 8, considering the system input variables, it is possible to evaluate the input-output pairs data through three-dimensional curves. In this case, in order to evaluate ANFIS results on training the parameters, three-dimensional data fitting curve of ANFIS controller through different input signals including IS1= $\Delta\omega_{SSSG}$, IS2= ΔP_{OWF}, IS3= ΔP_{WEF}, IS4= ΔP_{PV} with respect to output signal CS=IC are investigated which the results are provided in Figure 9.

From Figure 9, it is indicated that considering input combinations, there are different surfaces which are specified as controlling areas. In this case, the provided results show the independency of presented input variables with respect to evaluated sampling data. In order to design the ANFIS membership functions parameters, considering the MF epochs value as 10 and using the hybrid BPA-LSOT algorithm, the system training procedures are developed.

In order to evaluate the ANFIS system generalization manner through different sampling data, a cross validation (CV) scheme consisting of ten k fold and 290 input features are used which are developed through a set of If-Then rules for tuning the system MF functions. In the case of ANFIS training procedure, considering a set of 3-ph short circuit

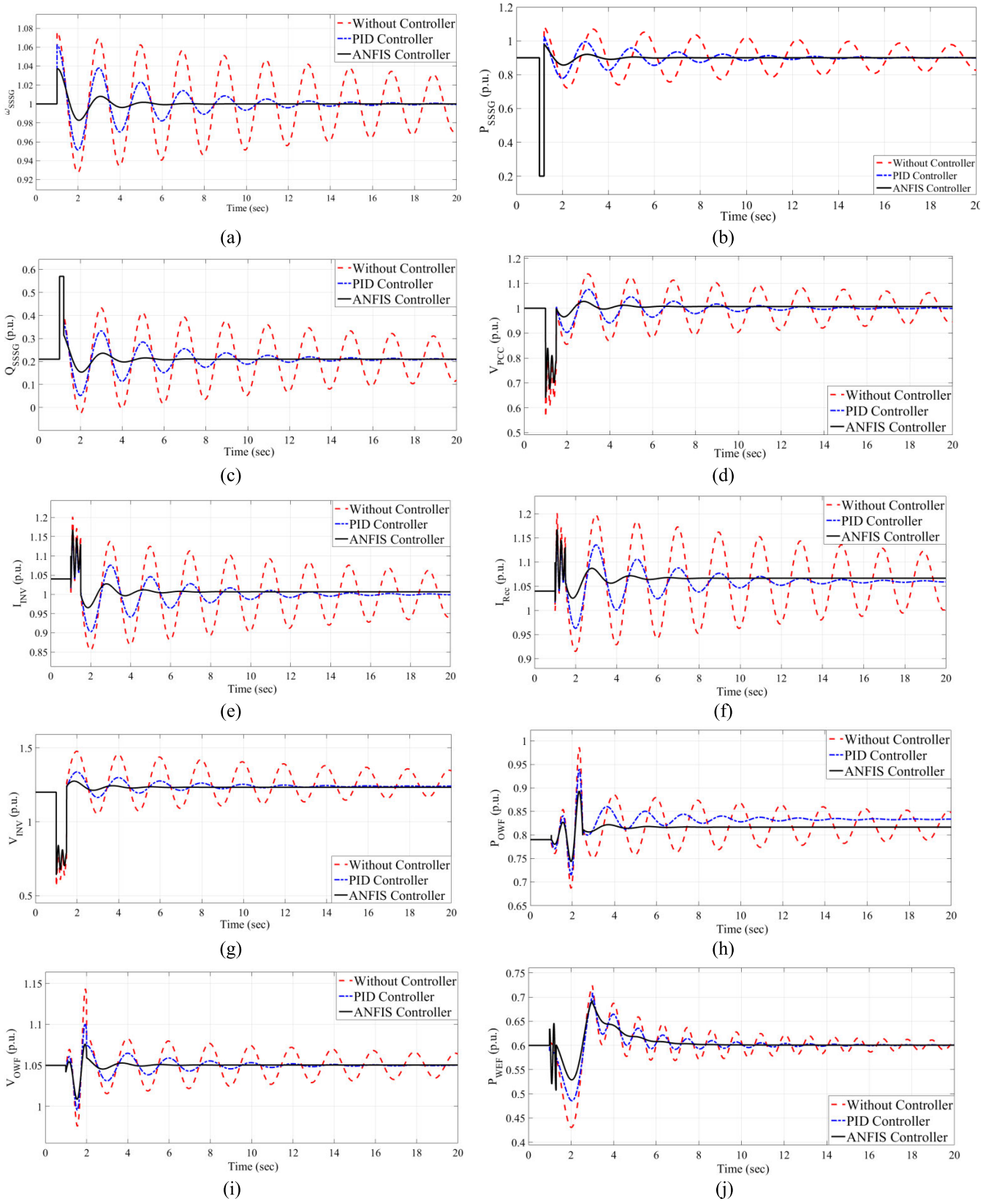

FIGURE 10. The system RESs dynamic oscillation with respect to short circuit fault event occurred at infinite bus location.

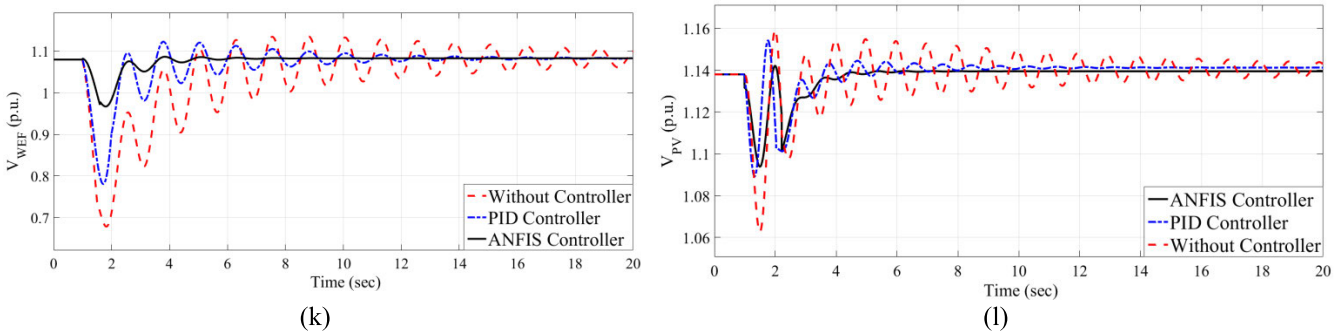

FIGURE 10. *(Continued.)* **The system RESs dynamic oscillation with respect to short circuit fault event occurred at infinite bus location.**

faults through provided different locations of the system, the RESs dynamic oscillations are evaluated and used as input data through ANFIS structure. The corresponding algorithm parameters after providing the system training procedure are evaluated as follows:

- Number of ANFIS nodes= 81, - Number of ANFIS linear data= 111, - Number of nonlinear data=19,

- Total number of data= 130, - Number of training pairs data= 21060, - Number of ANFIS fuzzy rules=345.

Based on provided ANFIS structure, the system accuracy is analyzed and tested using 10 fold CV scheme. During different evaluations through CV test scheme, the provided ANFIS structure error value estimated as 0.0141501 which means about 1.4% error within all of evaluated test cases. Test results present the effectiveness of the proposed ANFIS system with proper accuracy ratio through provided test data.

IV. SIMULATION STUDIES

In this section, considering the microgrid test system provided in Section II and the proposed PID and ANFIS damping controllers presented in Section III, the system dynamic behaviors through 3-phase short circuit fault events are investigated.

For this issue, considering the RESs *OP1*=13 m/s, *OP2*=3 m/s, PV output current IPV within solar radiation of 1000 W/m2 and diode reverse current ID=9.5 × 10.11, damping performance of proposed PID and ANFIS damping controllers are evaluated.

The system dynamic oscillations consisting of microgrid frequency response with and without the proposed ANFIS damping controller through 3-phase short circuit fault event at infinite bus are illustrated in Figure 10.

Based on Figure10, the first three diagrams from (a) to (c) presents the synchronous speed deviation ωSSSG, output active power PSSSG and output reactive power QSSSG, respectively. Also, Figure10(d)-(g) present the microgrid voltage at PCC point VPCC, the system dc current from rectifier side IINV, the system ac current from inverter side IRec, the system dc voltage from inverter side VINV, respectively. The system OWF output signals consist of the output active power POWF and the output voltage VOWF are presented in Figure10(h)-(i), respectively. Also, the system WEF output signals consist of the output active power PWEF and the output voltage VWEF are presented in Figure10(j)-(k), respectively. Finally, Figure10(l) presents the output dc voltage of the system PVs VPV.

A. COMPARISON STUDY OF THE PROPOSED SCHEME WITH RECENT STUDIES

From Figure10, considering three phase short circuit fault event occurred at t=1 s and cleared at t=1.2 s, the system dynamic oscillations within three different cases including (a) without activating damping controllers, (b) activating developed PID controller and (c) the proposed ANFIS-based damping controller are investigated. In this case, based on evaluating the percentages of RES output signal overshoots (OSH) and undershoots (USH), two online indexes are proposed which damping performance of the proposed controllers are evaluated. Comparative results of the proposed damping controllers with respect to developed OSH and USH online indexes through RES signals are illustrated in Table 3.

TABLE 3. Comparative results of two OSH and USH indexes through RES output signals.

RES Signals	OSH (%)			USH (%)		
	Without Controller	PID	ANFIS	Without Controller	PID	ANFIS
ω_{SSSG}	7.9%	6.1%	3.9%	7%	4.4%	1.8%
P_{SSSG}	27.8%	19%	8.7%	20%	12.5%	6%
Q_{SSSG}	210%	55%	9.5%	104%	31%	15%
V_{PCC}	13%	9%	3%	15%	10%	3%
I_{INV}	14.1%	5%	2.9%	23%	15.6%	7.3%
I_{Rec}	13.3%	7.5%	2.8%	16.5%	10.1%	1.9%
V_{INV}	25%	12.5%	4.2%	14.3%	4.3%	0.6%
P_{OWF}	2.1%	6.5%	10%	7%	1.1%	0.56%
V_{OWF}	9.5%	0.96%	0.31%	17%	0.41%	0.25%
P_{WEF}	22%	16%	12%	36%	20%	11%
V_{WEF}	28.8%	6.1%	1.1%	57%	17.5%	4.2%
V_{PV}	27%	19%	5.3%	36%	9.2%	3.4%

Also, in order to evaluate the effectiveness of the proposed scheme, a comprehensive comparison study is investigated between the proposed ANFIS approach and a few recent studies as summarized in Table 4. In the case of evaluating suitable results, considering the same fault scenario, the

system dynamic behavior and controllers damping performances are investigated as summarized in Table 4.

TABLE 4. Comparison of the proposed ANFIS scheme with a few recent techniques.

Ref	Damp Index (pu)	Cycles	Model-based	Complexity	Large Grids?
[1]	0.51	4	No	Medium	Yes
[2]	1.31	6	High	Medium	No
[3]	0.96	5	Medium	High	No
[4]	0.53	6	No	Medium	Yes
[6]	0.85	>10	High	Medium	Yes
[8]	0.71	8	Medium	High	No
[10]	0.55	9	High	High	No
[11]	0.76	8	Medium	High	No
[14]	0.58	>10	Medium	High	No
[19]	0.61	>10	Medium	Medium	Yes
[22]	0.89	6	No	Medium	No
Proposed ANFIS	**0.267**	**2**	**No**	**Medium**	**Yes**

From Table 4, the proposed ANFIS controller presents better results with specified parameters. The main major advantage is its no-model-based strategy to the system settings and medium complexity which resulted in its performance under a wide variety of applications. Also, in comparison, most other techniques require several cycles with a high dependency on the system model to control the oscillation. In this case, their performances highly depend on the system operational and topological conditions which in the case of changing operating points, updated adjustments are needed. Also, since an online approach based on wide area signal measurement is proposed, it can be easily used on different power systems with lower costs and complexities. Also, comparing with conventional PID, the proposed ANFIS damping controller presents better performances with proper damping ratio. It is indicated that without considering damping controller, the system RESs experience severe oscillations with poor damping ratio which are damped poorly through long-time durations. In this case, considering ANFIS-based damping controller through HVDC link, suitable damping performance with the most proper damping ratio is provided. In overall, the proposed ANFIS controller can be used through microgrids with HVDC links which based on designing parameters, proper damping performances with high damping ratios are achieved.

V. FURTHER DISCUSSIONS

In this section, some important issues related to provided controlling scheme are provided. Through modern power systems, inventing the inverter-based low inertia resources and developing power electronic AC/DC systems are known the most two important challenges within the power system stabilities. For this issue, considering the inverter-based resources, the system equivalent inertia is decreased which lead to transient instability issues through whole of power system. Also, the corresponding frequency response of these low-inertia systems are larger than allowable boundaries which provide the frequency transient instabilities through fault event scenarios. Therefore, in the case of developing the proposed scheme through low-inertia systems, it is important to evaluate the system transient and frequency responses to avoid large blackouts. In this case, the separation type of low-inertia systems within a set of stable microgrids still as an important issue which must be investigated. Also, through AC/DC-based power systems, considering the HVDC transmission lines provide more complexity through controlled islanding schemes. In this case, if this HVDC lines are considered as a boundary, the corresponding controlling system is becoming more complex. Therefore, investigating the performance of multiple HVDC links through provided controlled

TABLE 5. Microgrid parameters.

Base Values	V_{Base}=20/180/200/230 kV, S_{Base}=4×55.5=222 MVA, $\omega_{Base}= 2\pi f_{Base}$, f_{Base}=50 Hz,
SSSG Parameters	S_{SSSG}=4×55.5=222 MVA V=24 kV, Power Factore (PF)= 0.9 lagging, X_d''= 0.22 p.u., X_d'= 0.31 p.u., X_d= 1.83 p.u., X_l= 0.17 p.u, T_{do}'=7.9 s, T_{qo}'=1.1 s, T_{do}''=0.031 s, T_{qo}''=0.072 s, D=0 p.u, H=3.6 s, K_A=205, T_R=0.015 s, T_A=0.056 s, T_E=0.37 s, T_F=1.81 s, K_F=0.126 s, A_{EX}=0.0057, B_{EX}=1.078
PMSG Parameters	P_{PMSG}=2 MW, V=690 v, r_{sw}=0.041 p.u., X_{ls}= 0.0051 p.u., C_{DC}=0.16 p.u. X_{dw}=1.06 p.u., X_{qw}=0.078 p.u. X_{md}=0.58 p.u., i_m=1.61 p.u., H_{gw}=0.51 p.u., H_{hw}=2.51 p.u., K_{hgw}=0.31 p.u., D_{hgw}=0.051 p.u., K_{Pw}=10.21, K_{Iw}=30.1, τ_w=110 s, $\beta_{w\text{-}min}$=0 degree, $\beta_{w\text{-}max}$=30 degree, K_{w1}=0.011, T_{w1}=0.011 s, K_{w2}=0.011, T_{w2}=0.011 s, K_{w3}=0.12, T_{w3}=0.011 s, K_{w4}=0.011, T_{w4}=0.011 s,
Induction Generator Parameters	P_{IG}= 2 MW, V=690 V, r_{smr}=0.005 p.u, X_{smr}=0.0924 p.u. r_{rmr}=0.065 p.u., X_{rmr}=0.01 p.u., X_{mmr}=3.96 p.u., H_{gmr}=0.5 p.u., H_{hmr}=3.5 p.u., K_{hgmr}=0.15 p.u., D_{hgmr}=0.11 p.u., K_{pmr}=20.1, K_{Imr}=30.1, τ_{mr}=120 s, $\beta_{mr\text{-}min}$= 0 degree, $\beta_{mr\text{-}max}$= 30 degree,
HVDC Link Parameters	R_{DC}=0.051 p.u., L_{DC}=0.21 p.u., C_{DC}=0.61 p.u., C_I=0.31 p.u., C_R=0.61 p.u., T_R=0.11 s, K_R=1.05 p.u., T_I=0.11 s, K_I=1.01 p.u., $\alpha_{R\text{-}max}$=35 degree, $\alpha_{R\text{-}min}$=15 degree, $\gamma_{R\text{-}max}$=45 degree, $\gamma_{R\text{-}min}$=25 degree, $I_{C\text{-}max}$=0.11 p.u. , $I_{C\text{-}min}$=-0.11 p.u.
PV System Parameters	R_{DC_PV}=0.0056 p.u., L_{DC_PV}=0.031 p.u., C_{DC_PV}=0.21 p.u. T_{I_PV}=0.011 s, K_{I_PV}=1.01 p.u., γ_{I_PVmax}=25 degree, γ_{I_PVmin}=15 degree,

islanding in an interesting issue which can be evaluated though future studies.

VI. CONCLUSION

In this paper, an adaptive ANFIS damping controller developed for controlling and damping the microgrid dynamic oscillations equipped with renewable energy resources. In this case, considering four different RES types including the offshore wind farms, wave energy farms, photovoltaic arrays and small-scale synchronous generators connected through an HVDC link, the system damping performances evaluated. In the case of designing damping controllers, two different ANFIS and PID-based controllers were designed through HVDC link.

The proposed ANFIS controllers are based on linguistic fuzzy role for training and tuning the parameters. In this case, four electromechanical variables including SSSG speed deviations $\Delta\omega_{SSSG}$, wind farm active powers P_{OWF}, wave farm active powers P_{WEF} and PV active power P_{PV} used as input signal. In this case, the input signals are transformed into the linguistic variables used to ANFIS structure in which the corresponding fuzzification roles are learned. The corresponding ANFIS membership functions are similar to artificial neural network structures based on Sugeno algorithm, fuzzification roles are estimated. Also, in order to estimate damping parameters, using combined least-square and back-propagations gradient decent techniques as the main function, ANFIS membership functions were trained.

Based on evaluating input signals and controller parameters, proper controlling power in phase with the system dynamic oscillations were provided. Simulation results indicate effectiveness of the proposed model-based controller for damping the system dynamic oscillation through severe short circuit fault event. In this case, the proposed nonlinear ANFIS-based damping controller presents robust controlling performances which can be used as an adaptive damping controller through real-time evaluations.

APPENDIX

See Table 5.

CONFLICT OF INTEREST

On behalf of all authors, the corresponding author states that there is no conflict of interest.

REFERENCES

[1] Md. A. Islam, J. G. Singh, I. Jahan, M. S. H. Lipu, T. Jamal, R. M. Elavarasan, and L. Mihet-Popa, "Modeling and performance evaluation of ANFIS controller-based bidirectional power management scheme in plug-in electric vehicles integrated with electric grid," *IEEE Access*, vol. 9, pp. 166762–166780, 2021.

[2] M. M. Ismail and A. F. Bendary, "Smart battery controller using ANFIS for three phase grid connected PV array system," *Math. Comput. Simul.*, vol. 167, pp. 104–118, Jan. 2020.

[3] C. Rohmingtluanga, S. Datta, N. Sinha, T. S. Ustun, and A. Kalam, "ANFIS-based droop control of an AC microgrid system: Considering intake of water treatment plant," *Energies*, vol. 15, no. 19, p. 7442, Oct. 2022, doi: 10.3390/en15197442.

[4] M. Elsisi, M.-Q. Tran, K. Mahmoud, M. Lehtonen, and M. M. F. Darwish, "Robust design of ANFIS-based blade pitch controller for wind energy conversion systems against wind speed fluctuations," *IEEE Access*, vol. 9, pp. 37894–37904, 2021.

[5] H. M. Moghadam, M. Gheisarnejad, Z. Esfahani, and M.-H. Khooban, "A novel supervised control strategy for interconnected DFIG-based wind turbine systems: MiL validations," *IEEE Trans. Emerg. Topics Comput. Intell.*, vol. 5, no. 6, pp. 962–971, Dec. 2021.

[6] Y.-K. Wu, Y.-C. Wu, J.-S. Hong, L. H. Phan, and Q. D. Phan, "Probabilistic forecast of wind power generation with data processing and numerical weather predictions," *IEEE Trans. Ind. Appl.*, vol. 57, no. 1, pp. 36–45, Jan. 2021.

[7] S. A. Ibrahim, A. Nasr, and M. A. Enany, "Maximum power point tracking using ANFIS for a reconfigurable PV-based battery charger under non-uniform operating conditions," *IEEE Access*, vol. 9, pp. 114457–114467, 2021.

[8] K. R. Reddy and S. Meikandasivam, "Load flattening and voltage regulation using plug-in electric vehicle's storage capacity with vehicle prioritization using ANFIS," *IEEE Trans. Sustain. Energy*, vol. 11, no. 1, pp. 260–270, Jan. 2020.

[9] I. Sepehrirad, R. Ebrahimi, E. Alibeiki, and S. Ranjbar, "Intelligent differential protection scheme for controlled islanding of microgrids based on decision tree technique," *J. Control, Autom. Electr. Syst.*, vol. 31, no. 5, pp. 1233–1250, Oct. 2020, doi: 10.1007/s40313-020-00588-7.

[10] T. Aggab, M. Avila, P. Vrignat, and F. Kratz, "Unifying model-based prognosis with learning-based time-series prediction methods: Application to Li-ion battery," *IEEE Syst. J.*, vol. 15, no. 4, pp. 5245–5254, Jun. 2021.

[11] X. Tian, R. He, X. Sun, Y. Cai, and Y. Xu, "An ANFIS-based ECMS for energy optimization of parallel hybrid electric bus," *IEEE Trans. Veh. Technol.*, vol. 69, no. 2, pp. 1473–1483, Feb. 2020.

[12] M. Suhail, I. Akhtar, S. Kirmani, and M. Jameel, "Development of progressive fuzzy logic and ANFIS control for energy management of plug-in hybrid electric vehicle," *IEEE Access*, vol. 9, pp. 62219–62231, 2021.

[13] M. J. Alinezhad, M. Radmehr, and S. Ranjbar, "Adaptive wide area damping controller for damping inter-area oscillations considering high penetration of wind farms," *Int. Trans. Electr. Energy Syst.*, vol. 30, no. 6, Mar. 2020, doi: 10.1002/2050-7038.12392.

[14] S. Jha, B. Singh, and S. Mishra, "Control of ILC in an autonomous AC–DC hybrid microgrid with unbalanced nonlinear AC loads," *IEEE Trans. Ind. Electron.*, vol. 70, no. 1, pp. 544–554, Jan. 2023.

[15] Q. Zhou, D. Zhao, B. Shuai, Y. Li, H. Williams, and H. Xu, "Knowledge implementation and transfer with an adaptive learning network for real-time power management of the plug-in hybrid vehicle," *IEEE Trans. Neural Netw. Learn. Syst.*, vol. 32, no. 12, pp. 5298–5308, Dec. 2021.

[16] M. Rezaee, M. S. Moghadam, and S. Ranjbar, "Online estimation of power system separation as controlled islanding scheme in the presence of inter-area oscillations," *Sustain. Energy, Grids Netw.*, vol. 21, Mar. 2020, Art. no. 100306, doi: 10.1016/j.segan.2020.100306.

[17] J. Faraji, A. Ketabi, H. Hashemi-Dezaki, M. Shafie-Khah, and J. P. S. Catalão, "Optimal day-ahead self-scheduling and operation of prosumer microgrids using hybrid machine learning-based weather and load forecasting," *IEEE Access*, vol. 8, pp. 157284–157305, 2020.

[18] S. Ranjbar, M. Aghamohammadi, and F. Haghjoo, "A new scheme of WADC for damping inter-area oscillation based on CART technique and thevenine impedance," *Int. J. Electr. Power Energy Syst.*, vol. 94, pp. 339–353, Jan. 2018, doi: 10.1016/j.ijepes.2017.07.010.

[19] V. Hosseinnezhad, M. Shafie-Khah, P. Siano, and J. P. S. Catalão, "An optimal home energy management paradigm with an adaptive neuro-fuzzy regulation," *IEEE Access*, vol. 8, pp. 19614–19628, 2020.

[20] S. N. V. B. Rao, Y. V. P. Kumar, D. J. Pradeep, C. P. Reddy, A. Flah, H. Kraiem, and J. F. Al-Asad, "Power quality improvement in renewable-energy-based microgrid clusters using fuzzy space vector PWM controlled inverter," *Sustainability*, vol. 14, no. 8, p. 4663, Apr. 2022.

[21] S. N. V. B. Rao, Y. V. P. Kumar, M. Amir, and F. Ahmad, "An adaptive neuro-fuzzy control strategy for improved power quality in multi-microgrid clusters," *IEEE Access*, vol. 10, pp. 128007–128021, 2022.

[22] D. Çelik and M. E. Meral, "Multi-objective control scheme for operation of parallel inverter-based microgrids during asymmetrical grid faults," *IET Renew. Power Gener.*, vol. 14, no. 13, pp. 2487–2498, Oct. 2020.

[23] H. Ahmed and D. Çelik, "Sliding mode based adaptive linear neuron proportional resonant control of Vienna rectifier for performance improvement of electric vehicle charging system," *J. Power Sources*, vol. 542, Sep. 2022, Art. no. 231788.

[24] T. Surinkaew, R. Shah, S. M. Muyeen, N. Mithulananthan, K. Emami, and I. Ngamroo, "Novel control design for simultaneous damping of inter-area and forced oscillation," *IEEE Trans. Power Syst.*, vol. 36, no. 1, pp. 451–463, Jan. 2021.
[25] L. Wang and C.-N. Li, "Dynamic stability analysis of a tidal power generation system connected to an onshore distribution system," *IEEE Trans. Energy Convers.*, vol. 26, no. 4, pp. 1191–1197, Dec. 2011.
[26] L. Wang and J.-H. Liu, "Dynamic analysis of a grid-connected marine-current power generation system connected to a distribution system," *IEEE Trans. Power Syst.*, vol. 25, no. 4, pp. 1798–1805, Nov. 2010.
[27] *Modeling New Forms of Generation and Storage CIGRE*, document TF.01.10, Fifth Draft, Jun. 2000.
[28] M. E. Montilla-Djesus, D. Santos-Martin, S. Arnaltes, and E. D. Castron-uovo, "Optimal operation of offshore wind farms with line-commutated HVDC link connection," *IEEE Trans. Energy Convers.*, vol. 25, no. 2, pp. 504–513, Jun. 2010.
[29] K. R. Padiyar, *HVDC Power Transmission Systems*, 2nd ed. New Delhi: New Age International (P) Limited, 2002.
[30] M. A. Mahmud, H. R. Pota, and M. J. Hossain, "Dynamic stability of three-phase grid-connected photovoltaic system using zero dynamic design approach," *IEEE J. Photovolt.*, vol. 2, no. 4, pp. 564–571, Oct. 2012.
[31] C.-H. Lin, W.-L. Hsieh, C.-S. Chen, C.-T. Hsu, T.-T. Ku, and C.-T. Tsai, "Financial analysis of a large-scale photovoltaic system and its impact on distribution feeders," *IEEE Trans. Ind. Appl.*, vol. 47, no. 4, pp. 1884–1891, Jul. 2011.
[32] S. Ranjbar, M. R. Aghamohammadi, and F. Haghjoo, "Damping inter-area oscillation in power systems using local psss based on global control signals," *Tabriz J. Electr. Eng. (TJEE)*, vol. 47, no. 3, 2017.
[33] L. Wang, K.-H. Wang, W.-J. Lee, and Z. Chen, "Power-flow control and stability enhancement of four parallel-operated offshore wind farms using a line-commutated HVDC link," *IEEE Trans. Power Del.*, vol. 25, no. 2, pp. 1190–1202, Apr. 2010.
[34] M. Sugeno and G. T. Kang, "Structure identification of fuzzy model," *Fuzzy Sets Syst.*, vol. 28, no. 1, pp. 15–33, Oct. 1988.
[35] T. Amraee and S. Ranjbar, "Transient instability prediction using decision tree technique," *IEEE Trans. Power Syst.*, vol. 28, no. 3, pp. 3028–3037, Aug. 2013, doi: 10.1109/TPWRS.2013.2238684.
[36] M. Kumar and D. Garg, "Intelligent learning of fuzzy logic controllers via neural network and genetic algorithm," in *Proc. Japan-USA Symp. Flexible Automat. Denver (JUSFA)*, Denver, CO, USA, Jul. 2004, pp. 1–8.

ALIAKBAR HABIBI received the Associate degree in electrical engineering from Islamic Azad University, Nowshahr, in 2010, the bachelor's degree in electrical-power technology from the University of Maziar, Royan, in 2013, and the master's degree in electrical-power engineering from Islamic Azad University, Lahijan, in 2015. He is currently pursuing the Ph.D. degree in electrical-power engineering with Islamic Azad University, Nur. Since 2016, he has been teaching with the University of Povidengad, the University of Azad Chalous, the University of Sama, and the University of Allameh Hali Chalous.

BORZOU YOUSEFI received the master's degree in electrical engineering from the K. N. Toosi University of Technology, in 2016, the master's degree in electrical engineering from Mazandaran University, in 2017, and the Ph.D. degree in electrical engineering from the Islamic Azad University of Science and Research, Tehran, in 2018. He has been a member of the Academic Staff of Islamic Azad University, Nur Branch, since 2006. Before joining Islamic Azad University, he worked in the field of designing automation systems and precision instruments. His research interests include electric machines, reliability assessment in power systems, and restructuring in power systems.

ABDOLREZA NOORI SHIRAZI received the master's degree in electrical and electronic engineering from Semnan University, in 1999, the master's degree in electrical engineering from Islamic Azad University, Tehran South Branch, in 2003, and the Ph.D. degree in electrical engineering from Islamic Azad University, Science and Research Branch, in 2018. He has been a member of the Academic Staff of Islamic Azad University, Nur Branch, since 2013. His research interests include reactive power control in power systems, reliability assessment in power systems, and the exploitation of power systems.

MOHAMMAD REZVANI received the bachelor's degree in electrical engineering with a focus on control and the master's and Ph.D. degrees in electrical engineering with a focus on power systems from the K. N. Toosi University of Technology, in 2010, 2014, and 2016, respectively. He has been a member of the Academic Staff of the Islamic Azad University, Noor Branch, since 2010. His research interests include insulation and high pressure, electrical energy distribution systems, smart grid, and smart charging cars.